Electronic Supplementary Material (ESI) for Physical Chemistry Chemical Physics. This journal is © the Owner Societies 2022

Supplemental Material for "**Sum-frequency vibrational spectroscopy of methanol at interfaces due to Fermi resonance**"

Ren-Hui Zheng*[a] and Wen-Mei Wei*[b]

CONTENTS

[a] *Beijing National Laboratory for Molecular Sciences, State Key Laboratory for Structural Chemistry of Unstable and Stable Species, Institute of Chemistry, Chinese Academy of Sciences, Zhongguancun, Beijing 100190, P. R. China. E-mail: zrh@iccas.ac.cn*

[b] *School of Basic Medical Science, Anhui Medical University, Hefei, Anhui 230032, P. R. China. E-mail: cherrywwm@ustc.edu*

S1. Molecular structure of methanol, sum-frequency vibrational spectroscopy (SFVS) experimental arrangement and Euler angles

In Fig. S1(a), we show the molecular structure of methanol. At gas/liquid interfaces, the CH_3 group of methanol points to the gas phase. Thus, in the following computations and discussions, the C-O bond is taken to be along z axis in the molecular coordinates. In Fig. S1(b), we display the SFVS experimental arrangement in reflection, where the input IR and visible lights are on the same side of the normal and the output sum-frequency (SF) light is on the other side.[1] There is a relationship between the incident and reflection angles:[2] $k_2 sin\beta_2 + k_1 sin\beta_1 = k sin\beta$, where k_2, k_1 and k are the wave vectors of the IR, Vis and SF lights, respectively.

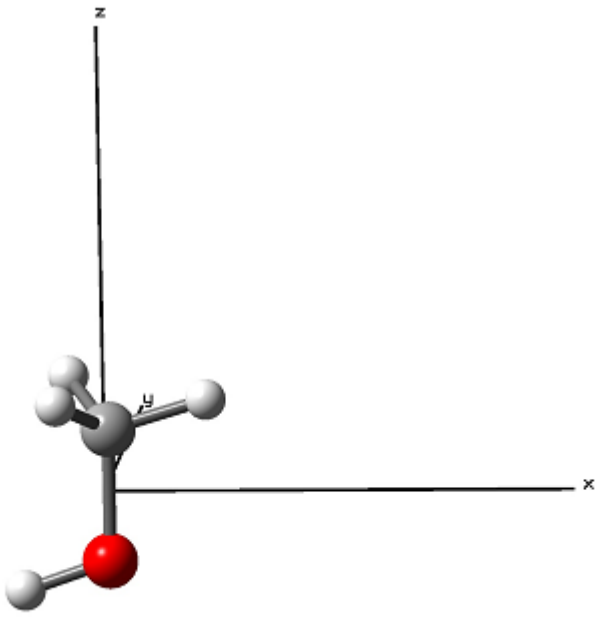

(a)

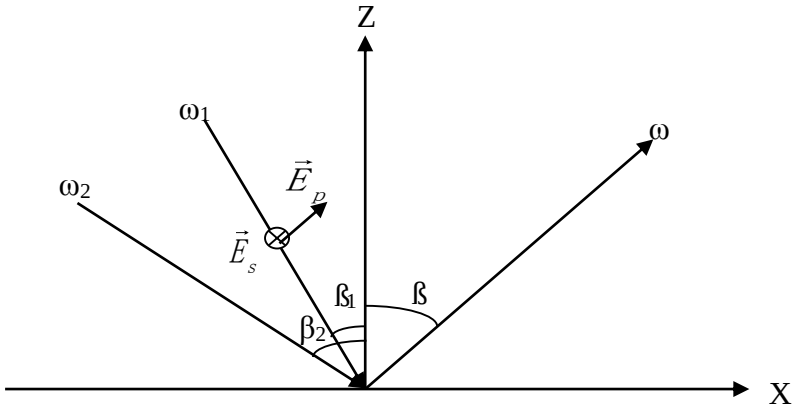

(b)

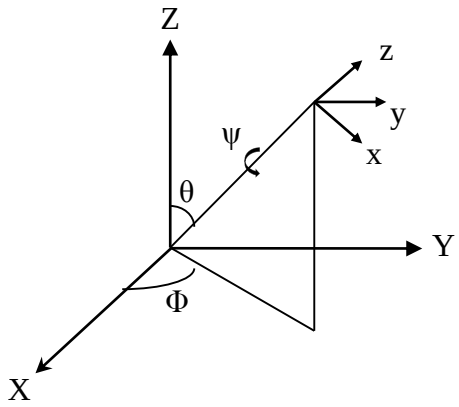

(c)

Fig. S1. (a) The molecular Structure of methanol, (b) SFVS experimental arrangement and (c) Euler angles relating the molecular coordinate (x,y,z) and the lab coordinate (X,Y,Z) systems.[3,4]

S2. Harmonic vibrational frequencies

Using density functional theory CAM-B3LYP/6-311++G**,[5] we optimize the molecular structure of methanol. In order to obtain accurate cubic and quartic force constants calculated by numerical differences, we use the keyword Opt=VeryTight, where the convergence threshold of maximum and root mean square (RMS) forces, and maximum and RMS displacements are 0.000002, 0.000001, 0.000006, 0.000004 a.u.,

respectively. Based on optimization, we calculate the harmonic frequencies. In Fig. S2, we show the displacements of the C-H stretching and H-C-H bending normal modes. Methanol belongs to C_s point group. The 3018 (totally symmetric mode) and 1490 cm^{-1} modes are symmetric vibrational modes with A′ symmetry, the 3140 and 1513 cm^{-1} modes also have A′ symmetry, and the 3070 (antisymmetric mode) and 1502 cm^{-1} modes are asymmetric vibrational modes with A″ symmetry (see Table S1).

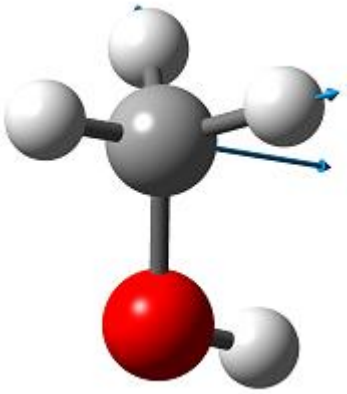

3140 cm^{-1}

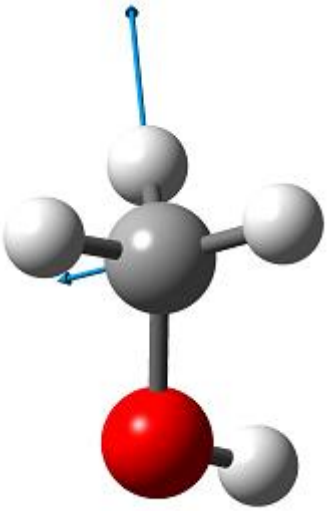

3070 cm^{-1}

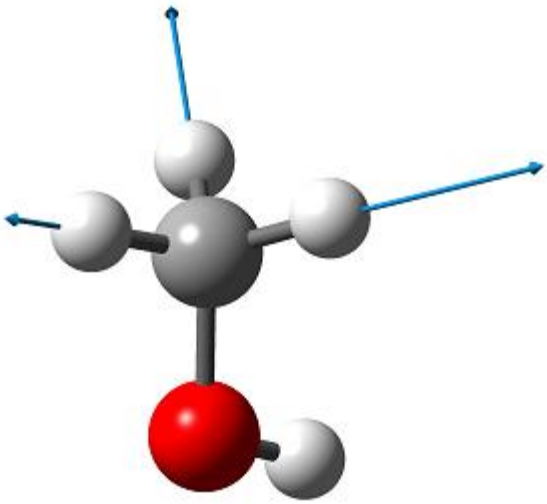

3018 cm^{-1}

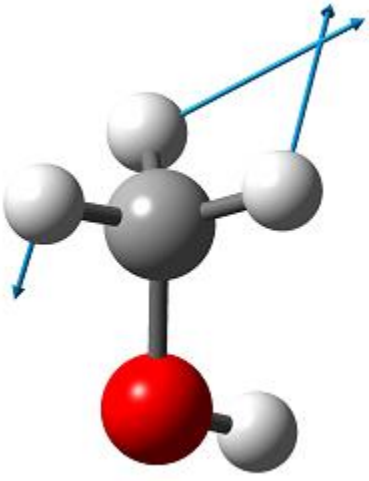

1513 cm^{-1}

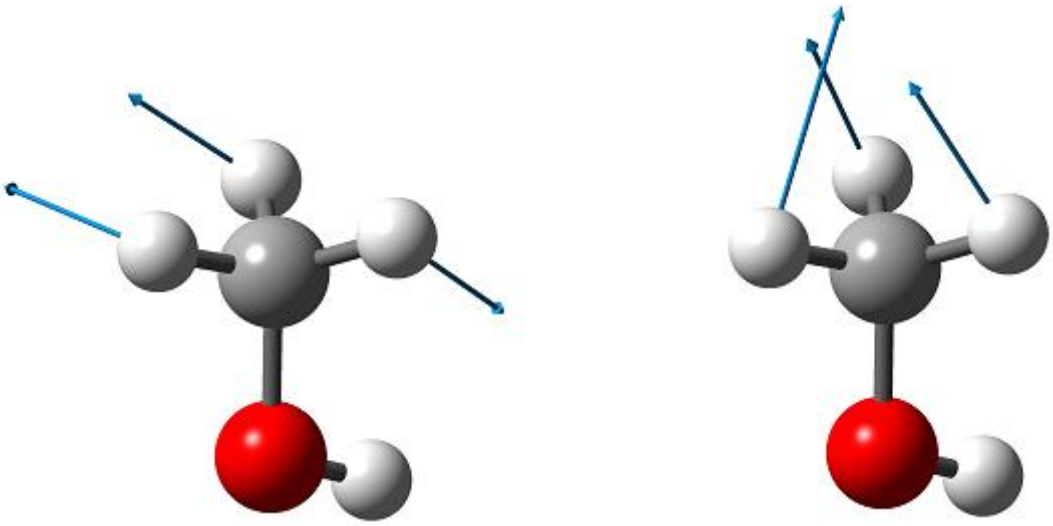

1502 cm^{-1} 1490 cm^{-1}

Fig. S2. The displacements of the 3140, 3070, 3018, 1513, 1502 and 1490 cm^{-1} vibrational modes.

S3. Anharmonic vibrational frequencies

In addition, we compute the anharmonic vibrational frequencies (see Table S1), which are better than the harmonic frequencies and agree well with the experimental ones. For example, the calculated C-H stretching and H-C-H bending anharmonic vibrational frequencies are 3005, 2943, 2834, 1478, 1465 and 1453 cm^{-1}, and the corresponding experimental ones are 3000, 2960, 2844, 1477, 1477 and 1455 cm^{-1}, respectively. The accurate anharmonic frequencies are the reason why we choose CAM-B3LYP. The anharmonic vibrational frequencies include the contributions of the quadratic, cubic and quartic force constants. The quadratic and cubic force constants have important influences on Fermi resonance (see eqn (13)). The quadratic force constants are calculated by the analytical method.

Table S1 Harmonic and anharmonic vibrational frequencies (cm^{-1}) calculated by CAM-B3LYP/6-311++G** and experimental vibrational frequencies for methanol.

Normal mode	Harm Freq[a]	Harm Freq[b]	Anh Freq[c]	Exp Freq[d]	Exp Freq[e]	Assignment[d]
Q0	3892A′	3873	3721	3681	3354	OH str
Q1	3140A′	3143	3005	3000	2980	CH_3 d-str
Q2	3070A″	3091	2943	2960	2945	CH_3 d-str
Q3	3018A′	3033	2834	2844	2833	CH_3 s-str
Q4	1513A′	1506	1478	1477	1477	CH_3 d-deform
Q5	1502A″	1491	1465	1477	1477	CH_3 d-deform
Q6	1490A′	1483	1453	1455	1450	CH_3 s-deform
Q7	1360A′	1361	1313	1345	1423	OH bend
Q8	1179A″	1180	1153	1165	1116	CH_3 rock
Q9	1091A′	1080	1066	1060	1045	CH_3 rock
Q10	1065A′	1054	1047	1033	1035	CO str
Q11	299A″	294	256	295	<400	Torsion

[a] in gas phase
[b] Polarizable Continuum Model (PCM)[6]
[c] in gas phase
[d] in gas phase[7]
[e] in liquid phase[8].

Using the second-order perturbation theory, the following vibrational energy can be obtained[9]

$$E(n) = V_0 + \hbar\left\{\hbar\xi_0 + \sum_{i=1}^{f}\left[\omega_i\left(n_i + \frac{1}{2}\right) + \hbar\sum_{j\geq i}^{f}\xi_{ij}\left(n_i + \frac{1}{2}\right)\left(n_j + \frac{1}{2}\right)\right]\right\}, \quad \text{(S1)}$$

where V_0 is the zero-order term of the potential energy expansion on the normal coordinates, $\omega_i = \sqrt{\lambda_i}$ (λ_i is the quadratic force constant), n_i (n_j) is the quantum number of the normal mode, ξ_0 and ξ_{ij} are the terms related to the cubic and quartic force constants, and Coriolis couplings.[9] ξ_0 contributes to the vibrational zero-point energy but not to the vibrational frequencies.[9,10] Therefore, the anharmonic vibrational frequencies for the fundamental, overtone and combination modes are respectively[9,10]

$$v_i = \omega_i + 2\xi_{ii} + \frac{1}{2}\sum_{j\neq i}\xi_{ij}, \quad \text{(S2)}$$

$$[2v_i] = 2\omega_i + 6\xi_{ii} + \sum_{j\neq i}\xi_{ij} = 2v_i + 2\xi_{ii}, \quad \text{(S3)}$$

$$[v_i v_j] = \omega_i + \omega_j + 2\xi_{ii} + 2\xi_{jj} + 2\xi_{ij} + \frac{1}{2}\sum_{l\neq i,j}(\xi_{il} + \xi_{jl}) = v_i + v_j + \xi_{ij}. \quad \text{(S4)}$$

ξ is called anharmonic X matrix in Gaussian computations[11]. ξ_{ii} is the diagonal term and ξ_{ij} is the non-diagonal one. Their detailed definitions can be found in ref. [9,10]. In Table S2, we list Coriolis couplings, the cubic and quartic force constants, and their total contributions to X matrix. From Table S2, we find that X matrix is symmetric, Coriolis contributions from the C-H stretching and H-C-H bending modes to X matrix are small, which may have few influences on SFVS, and the cubic and quartic force constants contributions to X matrix are relatively large, which may have important influences.

Table S2 Coriolis couplings, the cubic and quartic force constants, and their total contributions to X Matrix (cm^{-1}) in gas phase.

Coriolis	Q1	Q2	Q3	Q4	Q5	Q6
Q1	0.00	0.02	0.00	0.08	7.17	1.21

Q2	0.02	0.00	0.00	7.08	0.26	1.28
Q3	0.00	0.00	0.00	0.01	0.88	0.10
Q4	0.08	7.08	0.01	0.00	0.70	0.53
Q5	7.17	0.26	0.88	0.70	0.00	0.60
Q6	1.21	1.28	0.10	0.53	0.60	0.00
Cubic						
Q1	-109.27	-18.79	-48.61	3.47	42.22	44.08
Q2	-18.79	-69.59	-234.59	36.48	21.93	32.41
Q3	-48.61	-234.59	-50.67	15.33	6.20	18.92
Q4	3.47	36.48	15.33	-2.29	-5.73	-3.35
Q5	42.22	21.93	6.20	-5.73	-5.13	-9.07
Q6	44.08	32.41	18.92	-3.35	-9.07	-4.33
Quartic						
Q1	58.78	11.79	27.55	-8.26	-61.34	-53.15
Q2	11.79	36.27	125.10	-57.14	-24.31	-35.51
Q3	27.55	125.10	26.76	-39.11	-22.61	-33.10
Q4	-8.26	-57.14	-39.11	0.81	-1.26	0.70
Q5	-61.34	-24.31	-22.61	-1.26	0.59	2.03
Q6	-53.15	-35.51	-33.10	0.70	2.03	2.72
Total						
Q1	-50.48	-6.97	-21.06	-4.70	-11.94	-7.86
Q2	-6.97	-33.33	-109.49	-13.57	-2.11	-1.81

Q3	-21.06	-109.49	-23.91	-23.76	-15.54	-14.08
Q4	-4.70	-13.57	-23.76	-1.48	-6.29	-2.12
Q5	-11.94	-2.11	-15.54	-6.29	-4.54	-6.43
Q6	-7.86	-1.81	-14.08	-2.12	-6.43	-1.61

S4. Fermi matrix, eigenvectors and eigenvalues

According to eqn (S2)-(S4) and Table S1 and S2, the diagonal terms of Fermi matrix in eqn (13) can be:

$$\omega_{si} = \omega_i + 2\xi_{ii}, \tag{S5}$$

$$2\omega_{bj} = 2\omega_j + 6\xi_{jj}, \tag{S6}$$

$$\omega_{bj} + \omega_{bk} = \omega_j + \omega_k + 2\xi_{jj} + 2\xi_{kk} + 2\xi_{jk}. \tag{S7}$$

For the cubic force constants result in Fermi resonance, eqn (S5)-(S7) include the harmonic frequencies and the cubic force constants contributions to X matrix. Fermi matrix, eigenvalues and eigenvectors for Fermi wavefuntions $|n_F\rangle$ are listed in Table S3.

Table S3-1 Fermi matrix (cm^{-1})

H_F	Q1	Q2	Q3	Q4+Q5	Q4+Q6	Q5+Q6	2Q4	2Q5	2Q6
Q1	2922	0	0	0	-26.36	0	20.66	-61.34	-47.54
Q2	0	2931	0	-49.03	0	-60.40	0	0	0
Q3	0	0	2917	0	33.05	0	-65.85	-42.20	-87.89
Q4+Q5	0	-49.03	0	2989	0	0	0	0	0

Q4+Q6	-26.36	0	33.05	0	2982	0	0	0	0
Q5+Q6	0	-60.40		0	0	2955	0	0	0
2Q4	20.66	0	-65.85	0	0	0	3012	0	0
2Q5	-61.34	0	-42.20	0	0	0	0	2974	0
2Q6	-47.54	0	-87.89	0	0	0	0	0	2954

Table S3-2 Eigenvalues (cm^{-1}) of Fermi matrix

1_F	2_F	3_F	4_F	5_F	6_F	7_F	8_F	9_F
2809	2869	2877	2968	2973	2990	3033	3037	3079

Table S3-3 Eigenvectors of Fermi matrix

n_F	Q1	Q2	Q3	Q4+Q5	Q4+Q6	Q5+Q6	2Q4	2Q5	2Q6
1_F	0.3336	0.0000	0.6893	0.0000	-0.0807	0.0000	0.1902	0.3006	0.5296
2_F	0.0000	-0.7773	0.0000	-0.3174	0.0000	-0.5432	0.0000	0.0000	0.0000
3_F	-0.7522	0.0000	0.3905	0.0000	-0.3091	0.0000	0.3055	-0.3043	-0.0187
4_F	-0.0128	0.0000	0.1132	0.0000	-0.2861	0.0000	0.1780	0.6852	-0.6356
5_F	0.0000	-0.2127	0.0000	-0.6800	0.0000	0.7017	0.0000	0.0000	0.0000
6_F	0.0977	0.0000	-0.1249	0.0000	-0.8418	0.0000	-0.4846	-0.0439	0.1717
7_F	0.0000	0.5921	0.0000	-0.6610	0.0000	-0.4610	0.0000	0.0000	0.0000
8_F	0.5284	0.0000	-0.0576	0.0000	-0.2923	0.0000	0.5868	-0.4790	-0.2413
9_F	0.1847	0.0000	0.5837	0.0000	0.1486	0.0000	-0.5094	-0.3409	-0.4768

In order to consider the influences of Coriolis couplings and the quartic force constants on Fermi eigenvalues, we add the following energies:

$$\langle n_F | X_{C4} | n_F \rangle. \tag{S8}$$

X_{C4} is a matrix including the contributions of Coriolis couplings and the quartic force constants. Its diagonal terms are calculated with eqn (S5)-(S7), and with eqn (S2)-(S4), its non-diagonal terms between the fundamental, overtone and combination modes can be expressed into

$$v_i v_j = \frac{1}{2}\xi_{ij}$$

$$v_i[2v_j] = [2v_j]v_i = 2 * \frac{1}{2}\xi_{ij} = \xi_{ij},$$

$$v_i[v_j + v_k] = v_i[v_j] + v_i[v_k] = \frac{1}{2}(\xi_{ij} + \xi_{ik}),$$

$$[v_i + v_j][v_j + v_k] = v_i v_j + v_i v_k + v_j v_j + v_j v_k = \frac{1}{2}(\xi_{ij} + \xi_{ik} + \xi_{jk}),$$

$$[v_i + v_j][2v_k] = [2v_k]v_i + [2v_k]v_j = \xi_{ik} + \xi_{jk},$$

$$[v_i + v_j][2v_j] = [2v_j]v_i + [2v_j]v_j = \xi_{ij},$$

$$[2v_i][2v_j] = 2v_i[2v_j] = 2[2v_i]v_j = 2\xi_{ij} \tag{S9}$$

In Table S4-1, we present X_{C4} matrix, and in Table S4-2, we show the matrix calculated by eqn (S8), whose diagonal terms correspond to energy corrections from Coriolis couplings and the quartic force constants.

Table S4-1 Matrix (in cm^{-1}) including Coriolis couplings and the quartic force constants contributions

X_{C4}	Q1	Q2	Q3	Q4+Q5	Q4+Q6	Q5+Q6	2Q4	2Q5	2Q6
Q1	117.57	5.91	13.78	-31.17	-30.06	-53.05	-8.18	-54.16	-51.94

Q2	5.91	72.53	62.55	-37.05	-42.14	-29.13	-50.06	-24.05	-34.22
Q3	13.78	62.55	53.52	-30.41	-36.05	-27.37	-39.10	-21.73	-33.00
Q4+Q5	-31.17	-37.05	-30.41	1.71	1.65	1.65	-0.55	-0.55	3.86
Q4+Q6	-30.06	-42.14	-36.05	1.65	9.52	1.65	1.23	2.08	1.23
Q5+Q6	-53.05	-29.13	-27.37	1.65	1.65	11.90	0.67	2.64	2.64
2Q4	-8.18	-50.06	-39.10	-0.55	1.23	0.67	4.88	-1.11	2.46
2Q5	-54.16	-24.05	-21.73	-0.55	2.08	2.64	-1.11	3.56	5.27
2Q6	-51.94	-34.22	-33.00	3.86	1.23	2.64	2.46	5.27	16.32

Table S4-2 Coriolis couplings and the quartic force constants contributions (in cm^{-1}) to the Fermi eigenvalues

$\langle n_F \lvert X_{C4} \rvert n_F \rangle$	1_F	2_F	3_F	4_F	5_F	6_F	7_F	8_F	9_F
1_F	-16.2	17.5	12.3	4.7	-6.8	37.4	43.6	17.2	41.9
2_F	17.5	5.2	-38.7	-8.5	-1.5	-35.4	-42.4	18.9	-40.2
3_F	12.3	-38.7	37.2	4.7	6.8	-5.7	-5.0	-58.5	-18.3
4_F	4.7	-8.5	4.7	6.0	-0.7	4.5	14.6	2.8	17.6
5_F	-6.8	-1.5	6.8	-0.7	6.3	-12.6	-17.7	-9.4	-20.2
6_F	37.4	-35.4	-5.7	4.5	-12.6	3.6	29.5	19.2	28.6
7_F	43.6	-42.4	-5.0	14.6	-17.7	29.5	74.6	25.1	77.4
8_F	17.2	18.9	-58.5	2.8	-9.4	19.2	25.1	82.1	47.9
9_F	41.9	-40.2	-18.3	17.6	-20.2	28.6	77.4	47.9	92.6

S5. Electric dipole moment and polarizability derivatives

When computing the vibrational frequencies, we achieve the first-order electric dipole moment and polarizability derivatives analytically and the second-order derivatives numerically, which are listed in Table S5-S7. In Table S5, the anharmonic frequency calculated in gas phase for the C-H symmetric vibrational mode is 2843 cm^{-1}, and it is 2953 cm^{-1} with PCM computations, which is large and unreasonable. The reason is that the cubic and quartic force constants affecting the anharmonic frequencies are calculated numerically, and there may be problems when numerical differences are performed considering the solvent effect.

Table S5 The computational electric dipole moment derivatives (e Bohr) and the polarizability derivatives ($Bohr^3$) with respect to the normal modes.

Anh Freq (cm^{-1})	2834[a]	2953[b]	2943[a]	2957[b]	3005[a]	3004[b]
$\sqrt{\frac{\hbar}{2\omega_t}}\frac{\partial\langle G\|\mu_x\|G\rangle}{\partial Q_t}$	-0.0110	0.0088	0.0000	0.0000	-0.0213	0.0260
$\sqrt{\frac{\hbar}{2\omega_t}}\frac{\partial\langle G\|\mu_y\|G\rangle}{\partial Q_t}$	0.0000	0.0000	-0.0335	0.0349	0.0000	0.0000
$\sqrt{\frac{\hbar}{2\omega_t}}\frac{\partial\langle G\|\mu_z\|G\rangle}{\partial Q_t}$	-0.0336	-0.0355	0.0000	0.0000	0.0040	0.0030
$\sqrt{\frac{\hbar}{2\omega_t}}\frac{\partial\langle G\|\alpha_{xx}\|G\rangle}{\partial Q_t}$	0.8067	0.9588	0.0000	0.0000	-1.0813	-1.1058
$\sqrt{\frac{\hbar}{2\omega_t}}\frac{\partial\langle G\|\alpha_{xy}\|G\rangle}{\partial Q_t}$	0.0000	0.0000	0.6482	0.7094	0.0000	0.0000
$\sqrt{\frac{\hbar}{2\omega_t}}\frac{\partial\langle G\|\alpha_{xz}\|G\rangle}{\partial Q_t}$	0.2592	-0.2398	0.0000	0.0000	0.5310	-0.5903

$\sqrt{\frac{\hbar}{2\omega_t}}\frac{\partial\langle G\vert\alpha_{yy}\vert G\rangle}{\partial Q_t}$	1.3795	1.4493	0.0000	0.0000	0.2926	0.4027
$\sqrt{\frac{\hbar}{2\omega_t}}\frac{\partial\langle G\vert\alpha_{yz}\vert G\rangle}{\partial Q_t}$	0.0000	0.0000	0.8282	-0.8667	0.0000	0.0000
$\sqrt{\frac{\hbar}{2\omega_t}}\frac{\partial\langle G\vert\alpha_{zz}\vert G\rangle}{\partial Q_t}$	0.6962	0.7426	0.0000	0.0000	-0.0826	-0.0525

[a] in gas phase
[b] PCM

Table S6 The computational second-order electric dipole moment derivatives $\sqrt{\frac{\hbar}{2\omega_{bj}}}\sqrt{\frac{\hbar}{2\omega_{bk}}}\frac{\partial^2\langle G\vert\mu_\kappa\vert G\rangle}{\partial Q_{bj}\partial Q_{bk}}$ $(\kappa = x, y, z)$ (e Bohr) with respect to the normal modes in gas phase. Note that the diagonal terms are multiplied by $\frac{\sqrt{2}}{2}$.

x	Q4	Q5	Q6
Q4	-0.0020	0.0000	0.0010
Q5	0.0000	0.0008	0.0000
Q6	0.0010	0.0000	-0.0003
y			
Q4	0.0000	0.0017	0.0000
Q5	0.0017	0.0000	-0.0007
Q6	0.0000	-0.0007	0.0000
z			
Q4	-0.0025	0.0000	-0.0012
Q5	0.0000	-0.0020	0.0000
Q6	-0.0012	0.0000	-0.0038

Table S7 The computational second-order polarizability derivatives $\sqrt{\frac{\hbar}{2\omega_{bj}}}\sqrt{\frac{\hbar}{2\omega_{bk}}}\frac{\partial\langle G\vert\alpha_{\sigma\rho}\vert G\rangle}{\partial Q_{bj}\partial Q_{bk}}$ $(\sigma, \rho = x, y, z)$ (Bohr^3) with respect to the normal modes in gas phase. Note that the diagonal terms are multiplied by $\frac{\sqrt{2}}{2}$.

xx	Q4	Q5	Q6
Q4	0.0816	0.0000	-0.0374
Q5	0.0000	0.1009	0.0000
Q6	-0.0374	0.0000	0.0707
xy			

Q4	0.0000	0.0069	0.0000
Q5	0.0069	0.0000	0.0083
Q6	0.0000	0.0083	0.0000
xz			
Q4	0.0534	0.0000	0.0388
Q5	0.0000	-0.0257	0.0000
Q6	0.0388	0.0000	-0.0277
yy			
Q4	0.1076	0.0000	0.0083
Q5	0.0000	0.1108	0.0000
Q6	0.0083	0.0000	0.0579
yz			
Q4	0.0000	-0.0236	0.0000
Q5	-0.0236	0.0000	0.0817
Q6	0.0000	0.0817	0.0000
zz			
Q4	0.1098	0.0000	0.0252
Q5	0.0000	0.1354	0.0000
Q6	0.0252	0.0000	0.1446

S6. Lorentz local field correction factors

Before calculating Lorentz local field correction factors for methanol, we compute them with the point-dipole model[12,13] (see eqn (4)-(6)) as a function of Z_0 that is the distance of molecule from the substrate (see Fig. S3). In Fig. S3, we find that L_{xx} (L_{yy}) is larger than one and L_{zz} is smaller than one. In the computations, all the parameters are the same as those in Fig. 1 of ref. [13]. After comparison, we find that there is a small mistake in Fig. 1 of ref. [13]: L_{xx}(L_{yy}) and L_{zz} are swapped.

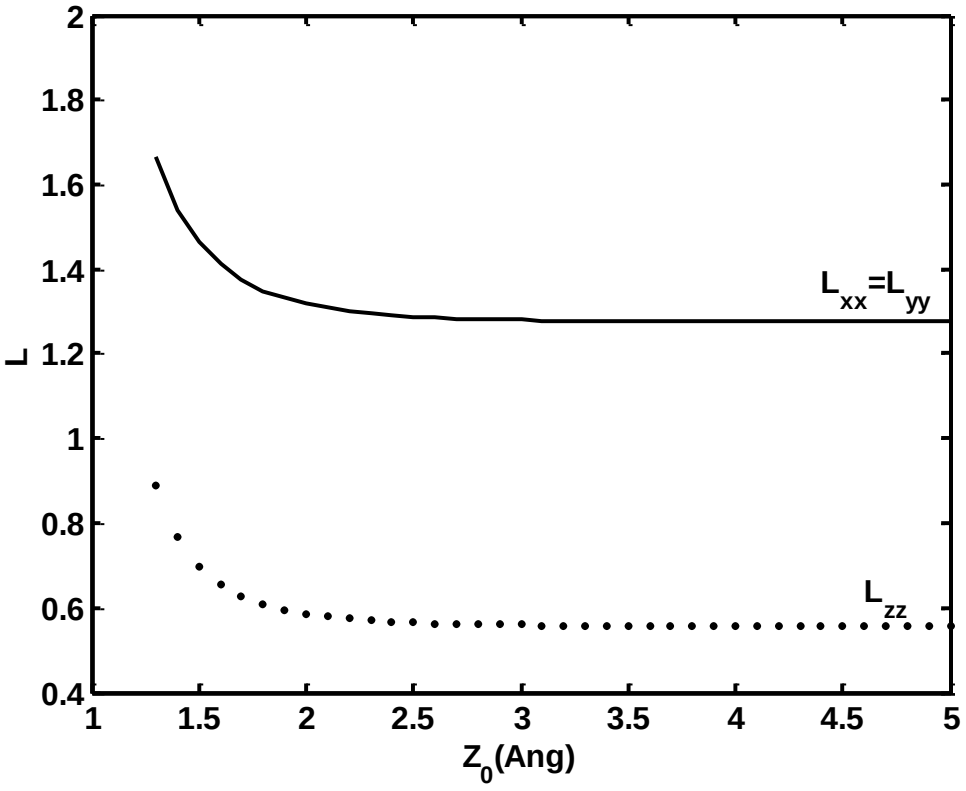

Fig. S3. Lorentz local field correction factors computed with the point-dipole model as a function of Z_0 that is the distance of molecule from the substrate when the lattice constant $a = 5$ Å , molecular polarizabilities $\alpha_{xx}(\alpha_{yy}) = 6$ Å^3 and $\alpha_{zz} = 11$ Å^3 for the adsorbed molecule, and the dielectric constant $\epsilon = 10$ for the substrate.

Then we compute the polarizabilities and dielectric constants for methanol when the light wavelengths are 3534 nm (2830 cm^{-1}), 532 nm and 462 nm, respectively. The lattice constant is taken to be the distance between the mass centers of methanol dimer, which is calculated by adding Petersson-Frisch dispersion.[14] For we study pure methanol liquids, the distance of molecule from substrate $Z_0 = \frac{a}{2}$. The twist and in-plane rotation angles are isotropic (see Fig. 1). Thus, the relationship between the macroscopic and microscopic polarizabilities can be

$$\alpha_{XX}(\alpha_{YY}) = \frac{1}{4}(1 + \langle cos^2\theta \rangle)\left(\alpha_{xx} + \alpha_{yy}\right) + \frac{1}{2}(1 - \langle cos^2\theta \rangle)\alpha_{zz}, \quad \text{(S10)}$$

$$\alpha_{ZZ} = \frac{1}{2}(1 - \langle cos^2\theta \rangle)\left(\alpha_{xx} + \alpha_{yy}\right) + \langle cos^2\theta \rangle)\alpha_{zz}. \quad \text{(S11)}$$

The calculated Lorentz local field correction factors are presented in Table S8. In the above computations, we apply PCM when the solvent effect is considered. All the computations are done with Gaussian 16 software package.[11]

Table S8 The calculated polarizabilities (a.u.) in molecular (lowercase for subscript) and the laboratory (uppercase for subscript) coordinates, dielectric constants ϵ, ρ (see eqn (7)), ξ_I (see eqn (6)), lattice constants a (Å), and the Lorentz local field correction factors *L* when the light wavelengths are 3534 nm, 532 nm and 462 nm, respectively.

Phase	In gas phase			PCM		
Wavelength	3534	532	462	3534	532	462
α_{xx}	18.35	18.80	18.96	19.19	19.67	19.84
α_{yy}	17.76	18.27	18.46	18.76	19.31	19.51
α_{zz}	19.85	20.37	20.55	20.76	21.32	21.52
$\alpha_{XX}(\alpha_{YY})$	18.50	18.99	19.17	19.42	19.95	20.14
α_{ZZ}	18.96	19.46	19.63	19.87	20.41	20.60
ϵ	1.517	1.531	1.536	1.542	1.557	1.562
ρ	0.2054	0.2097	0.2112	0.2133	0.2179	0.2195
ξ_I	0.6320			0.6320		
a	3.198			3.260		
$L_{XX}(L_{YY})$	1.638	1.667	1.678	1.615	1.643	1.653
L_{ZZ}	0.5444	0.5380	0.5358	0.5693	0.5628	0.5606
L_{XXZ}[a]	1.554			1.546		
L_{XZX}[a]	1.511			1.502		
L_{ZXX}[a]	1.496			1.487		
L_{ZZZ}[a]	0.1773			0.1796		

[a]$L_{IJK} = L_{II}L_{JJ}L_{KK}\ (I,J,K = X,Z)$

S7. Molecular dynamics simulation

The method of generating the force field parameters of methanol can be found in ref. 15. 1000 methanol molecules are built in simulation box using Gromacs program.[16] The simulation temperature is 298 K. First, we minimize the system with a steepest descent algorithm. Second, the simulation system is equilibrated with NPT for 1 ns. The equilibrated box is cubic and the box size is 40. 5782 Å. Third, we lengthen the Z direction to 81.1564 Å to add a vacuum and generate the methanol gas/liquid interfaces, and then the system is equilibrated with NVT for 1 ns. Last, 1ns NVT simulation is done to obtain the trajectory that is applied to calculate distributions. In the simulation, the time step is taken to be 1 fs, and we treat the long-range electrostatic interactions using Ewald summation.[17] In Fig. S4, we plot the density of methanol along the Z axis. The bulk density is about 810 kg/m^3, and the experimental one is 790 kg/m^3 with molecular density of 1.49×10^{28} m^{-3}. The theoretical density is close to experimental one. The molecules with the density ranging from 10% to 90% of the bulk system are taken as the gas/liquid interfaces.

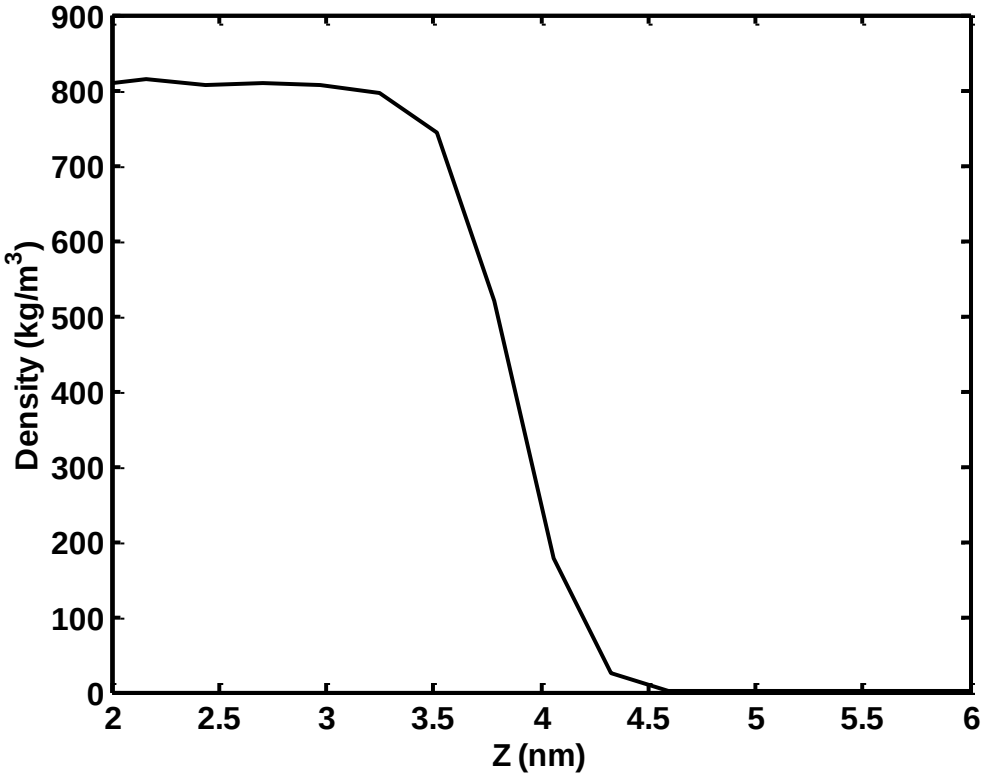

Fig. S4. Density of methanol along the Z axis at gas/liquid interfaces.

S8. Two vibrational modes model for Fermi resonance

In 2011, Ishiyama et al. presented the formulas of Fermi resonance for two vibrational modes of methanol using the first-order perturbation.[18] However, the two eigenstates deduced by them are not orthogonal or normalized (see eqn (B6a) in ref. 18). Here, we derive the formulas again. When there are two vibrational modes where one is the stretching mode and the other is the bending mode, Hamiltonian in eqn (10) can be simplified into

$$H = \hbar\omega_{si}|1_{si}\rangle\langle 1_{si}| + 2\hbar\omega_{bj}|2_{bj}\rangle\langle 2_{bj}| + \hbar V_{ij}(|1_{si}\rangle\langle 2_{bj}| + |2_{bj}\rangle\langle 1_{si}|)]. \qquad \text{(S12)}$$

The secular equation for the eigenvalues $\omega^{\pm}$ is

$$\begin{vmatrix} \hbar(\omega_{si} - \omega^{\pm}) & \hbar V_{ij} \\ \hbar V_{ij} & \hbar(2\omega_{bj} - \omega^{\pm}) \end{vmatrix} = 0. \qquad \text{(S13)}$$

Solving eqn (S13), we obtain

$$\omega^{\pm} = \frac{\omega_{si}+2\omega_{bj}}{2} \pm \sqrt{(\frac{\omega_{si}-2\omega_{bj}}{2})^2 + V_{ij}^2}, \tag{S14}$$

and the eigenvectors are respectively

$$c_1^{\pm} = \frac{2\omega_{b2}-\omega^{\pm}}{\sqrt{(2\omega_{b2}-\omega^{\pm})^2+V_{ij}^2}}, \tag{S15}$$

$$c_2^{\pm} = \frac{V_{ij}}{\sqrt{(2\omega_{b2}-\omega^{\pm})^2+V_{ij}^2}}. \tag{S16}$$

Fermi wavefunctions $|n_F^{\pm}\rangle = c_1^{\pm}|1_{si}\rangle + c_2^{\pm}|2_{bj}\rangle$ are orthogonal and normalized. When the coupling is small, $|2\omega_{bj} - \omega_{si}| \gg |V_{ij}|$. Using Taylor expansion, eqn (S14)-(S16) are rewritten as

(1) $\omega_{si} > 2\omega_{bj}$

$$\omega^{+} \approx \omega_{si} + \frac{V_{ij}^2}{\omega_{si}-2\omega_{bj}},\ \omega^{+} \approx \omega_{si}, \tag{S17}$$

$$\omega^{-} \approx 2\omega_{bj} - \frac{V_{ij}^2}{\omega_{si}-2\omega_{bj}},\ \omega^{-} \approx 2\omega_{bj}, \tag{S18}$$

$$c_1^{+} = -1 + \frac{V_{ij}^2}{2(\omega_{si}-2\omega_{bj})^2} \approx -1, \tag{S19}$$

$$c_2^{+} \approx -\frac{V_{ij}}{(\omega_{si}-2\omega_{bj})}, \tag{S20}$$

$$c_1^{-} \approx \frac{|V_{ij}|}{\omega_{si}-2\omega_{bj}}, \tag{S21}$$

$$c_2^{-} = \frac{-V_{ij}}{\sqrt{(2\omega_{bj}-\omega^{-})^2+V_{ij}^2}} \approx \frac{-V_{ij}}{\sqrt{V_{ij}^2}} = \frac{-V_{ij}}{|V_{ij}|} = \begin{cases} -1 & V_{ij} > 0 \\ 1 & V_{ij} < 0. \\ 0 & V_{ij} = 0 \end{cases} \tag{S22}$$

The orthogonal condition is satisfied for the above eigenvectors:

$$c_1^{+}c_1^{-} + c_2^{+}c_2^{-} \approx -\frac{|V_{ij}|}{\omega_{si}-2\omega_{bj}} + \frac{V_{ij}}{(\omega_{si}-2\omega_{bj})}\frac{V_{ij}}{|V_{ij}|} = 0. \tag{S23}$$

Hence, eq. (9) can be

$$\beta_{\sigma\rho\kappa}^{+} = \frac{1}{\hbar}\Big(\sqrt{\frac{\hbar}{2\omega_{si}}}\frac{\partial\langle G|\alpha_{\sigma\rho}|G\rangle}{\partial Q_{si}} + \frac{1}{2}\frac{V_{ij}}{\omega_{si}-2\omega_{bj}}\frac{\sqrt{2}\hbar}{2\omega_{bj}}\frac{\partial^2\langle G|\alpha_{\sigma\rho}|G\rangle}{\partial Q_{bj}^2}\Big) \times$$
$$\Big(\sqrt{\frac{\hbar}{2\omega_{si}}}\frac{\partial\langle G|\mu_{\kappa}|G\rangle}{\partial Q_{si}} + \frac{1}{2}\frac{V_{ij}}{\omega_{si}-2\omega_{bj}}\frac{\sqrt{2}\hbar}{2\omega_{bj}}\frac{\partial^2\langle G|\mu_{\kappa}|G\rangle}{\partial Q_{bj}^2}\Big)\frac{1}{\omega_2-\omega^{+}+i\Gamma_t}, \tag{S24}$$

$$\beta_{\sigma\rho\kappa}^{-} = \frac{1}{\hbar}\Big(\frac{-V_{ij}}{2|V_{ij}|}\frac{\sqrt{2}\hbar}{2\omega_{bj}}\frac{\partial^2\langle G|\alpha_{\sigma\rho}|G\rangle}{\partial Q_{bj}^2} + \frac{|V_{ij}|}{\omega_{si}-2\omega_{bj}}\sqrt{\frac{\hbar}{2\omega_{si}}}\frac{\partial\langle G|\alpha_{\sigma\rho}|G\rangle}{\partial Q_{si}}\Big) \times$$

$$\left(\frac{-V_{ij}}{2|V_{ij}|}\frac{\sqrt{2}\hbar}{2\omega_{bj}}\frac{\partial^2\langle G|\mu_\kappa|G\rangle}{\partial Q_{bj}^2}+\frac{|V_{ij}|}{\omega_{si}-2\omega_{bj}}\sqrt{\frac{\hbar}{2\omega_{si}}}\frac{\partial\langle G|\mu_\kappa|G\rangle}{\partial Q_{si}}\right)\frac{1}{\omega_2-\omega^-+i\Gamma_s}. \quad \text{(S25)}$$

(2) $\omega_{si}<2\omega_{bj}$

In this case, the corresponding eigenvalues $\omega^{r\pm}=\omega^{\mp}$. Therefore, molecular hyperpolarizabilities $\beta_{\sigma\rho\kappa}^{r+}=\beta_{\sigma\rho\kappa}^{-}$ and $\beta_{\sigma\rho\kappa}^{r-}=\beta_{\sigma\rho\kappa}^{+}$.

S9. The relationships between macroscopic and molecular hyperpolarizabilities

Through Euler angles θ (tilt angle), ψ (twist angle) and Φ (in-plane rotation angle), molecular hyperpolarizabilities are related to those in the laboratory coordinates. At interfaces, when the distribution of Φ angle is isotropic, the relationships between macroscopic and molecular hyperpolarizabilities are given by[3]

$$\chi_{zzz}=N_s\times$$
$$\left\{\begin{array}{l}\langle cos^3\theta\rangle(\beta_{zzz})\\ +\langle sin\theta sin\psi\rangle(\beta_{yzz}+\beta_{zyz}+\beta_{zzy})\\ -\langle sin\theta cos\psi\rangle(\beta_{xzz}+\beta_{zxz}+\beta_{zzx})\\ +\langle sin^2\theta cos\theta sin^2\psi\rangle(\beta_{yyz}+\beta_{yzy}+\beta_{zyy})\\ +\langle sin^2\theta cos\theta cos^2\psi\rangle(\beta_{xxz}+\beta_{xzx}+\beta_{zxx})\\ -\langle sin^2\theta cos\theta sin\psi cos\psi\rangle(\beta_{xyz}+\beta_{xzy}+\beta_{yxz}+\beta_{yzx}+\beta_{zxy}+\beta_{zyx})\\ +\langle sin^3\theta sin\psi\rangle(\beta_{xxy}+\beta_{xyx}+\beta_{yxx}-\beta_{yzz}-\beta_{zyz}-\beta_{zzy})\\ +\langle sin^3\theta cos\psi\rangle(\beta_{xzz}+\beta_{zxz}+\beta_{zzx}-\beta_{xyy}-\beta_{yxy}-\beta_{yyx})\\ +\langle sin^3\theta sin^3\psi\rangle(\beta_{yyy}-\beta_{xxy}-\beta_{xyx}-\beta_{yxx})\\ +\langle sin^3\theta cos^3\psi\rangle(-\beta_{xxx}+\beta_{xyy}+\beta_{yxy}+\beta_{yyx})\end{array}\right\}, \quad \text{(S26)}$$

$$\chi_{zxx}=\frac{1}{2}N_s\times\left\{\begin{array}{l}\langle sin^2\theta cos\theta\rangle(\beta_{zzz})+\langle cos\theta\rangle(\beta_{zxx}+\beta_{zyy})\\ -\langle sin^2\theta cos\theta sin^2\psi\rangle(\beta_{yyz}+\beta_{yzy}+\beta_{zyy})\\ -\langle sin^2\theta cos\theta cos^2\psi\rangle(\beta_{xxz}+\beta_{xzx}+\beta_{zxx})\\ +\langle sin^2\theta cos\theta sin\psi cos\psi\rangle(\beta_{xyz}+\beta_{xzy}+\beta_{yxz}+\beta_{yzx}+\beta_{zxy}+\beta_{zyx})\\ +\langle sin\theta sin\psi\rangle(\beta_{yyy}+\beta_{yxx}-\beta_{zyz}-\beta_{zzy})\\ +\langle sin\theta cos\psi\rangle(-\beta_{xxx}+\beta_{xyy}+\beta_{zxz}+\beta_{zzx})\\ +\langle sin^3\theta sin\psi\rangle(-\beta_{xxy}-\beta_{xyx}-\beta_{yxx}+\beta_{yzz}+\beta_{zyz}+\beta_{zzy})\\ +\langle sin^3\theta cos\psi\rangle(\beta_{xyy}+\beta_{yxy}+\beta_{yyx}-\beta_{xzz}-\beta_{zxz}-\beta_{zzx})\\ +\langle sin^3\theta sin^3\psi\rangle(-\beta_{yyy}+\beta_{xxy}+\beta_{xyx}+\beta_{yxx})\\ +\langle sin^3\theta cos^3\psi\rangle(\beta_{xxx}-\beta_{xyy}-\beta_{yxy}-\beta_{yyx})\end{array}\right\}, \quad \text{(S27)}$$

$$\chi_{XZX} = \frac{1}{2}N_s \times$$

$$\begin{Bmatrix} \langle sin^2\theta cos\theta\rangle(\beta_{zzz}) + \langle cos\theta\rangle(\beta_{xzx} + \beta_{yzy}) \\ -\langle sin^2\theta cos\theta sin^2\psi\rangle(\beta_{yyz} + \beta_{yzy} + \beta_{zyy}) \\ -\langle sin^2\theta cos\theta cos^2\psi\rangle(\beta_{xxz} + \beta_{xzx} + \beta_{zxx}) \\ +\langle sin^2\theta cos\theta sin\psi cos\psi\rangle(\beta_{xyz} + \beta_{xzy'} + \beta_{yxz} + \beta_{yzx} + \beta_{zxy} + \beta_{zyx}) \\ +\langle sin\theta sin\psi\rangle(\beta_{yyy} + \beta_{xyx} - \beta_{yzz} - \beta_{zzy}) \\ +\langle sin\theta cos\psi\rangle(-\beta_{xxx} - \beta_{yxy} + \beta_{xzz} + \beta_{zzx}) \\ +\langle sin^3\theta sin\psi\rangle(-\beta_{xxy} - \beta_{xyx} - \beta_{yxx} + \beta_{yzz} + \beta_{zyz} + \beta_{zzy}) \\ +\langle sin^3\theta cos\psi\rangle(\beta_{xyy} + \beta_{yxy} + \beta_{yyx} - \beta_{xzz} - \beta_{zxz} - \beta_{zzx}) \\ +\langle sin^3\theta sin^3\psi\rangle(-\beta_{yyy} + \beta_{xxy} + \beta_{xyx} + \beta_{yxx}) \\ +\langle sin^3\theta cos^3\psi\rangle(\beta_{xxx} - \beta_{xyy} - \beta_{yxy} - \beta_{yyx}) \end{Bmatrix}, \quad \text{(S28)}$$

$$\chi_{XXZ} = \frac{1}{2}N_s \times$$

$$\begin{Bmatrix} \langle sin^2\theta cos\theta\rangle(\beta_{zzz}) + \langle cos\theta\rangle(\beta_{xxz} + \beta_{yyz}) \\ -\langle sin^2\theta cos\theta sin^2\psi\rangle(\beta_{yyz} + \beta_{yzy} + \beta_{zyy}) \\ -\langle sin^2\theta cos\theta cos^2\psi\rangle(\beta_{xxz} + \beta_{xzx} + \beta_{zxx}) \\ +\langle sin^2\theta cos\theta sin\psi cos\psi\rangle(\beta_{xyz} + \beta_{xzy} + \beta_{yxz} + \beta_{yzx} + \beta_{zxy} + \beta_{zyx}) \\ +\langle sin\theta sin\psi\rangle(\beta_{yyy} + \beta_{xxy} - \beta_{yzz} - \beta_{zyz}) \\ +\langle sin\theta cos\psi\rangle(-\beta_{xxx} - \beta_{yyx} + \beta_{xzz} + \beta_{zxz}) \\ +\langle sin^3\theta sin\psi\rangle(-\beta_{xxy} - \beta_{xyx} - \beta_{yxx} + \beta_{yzz} + \beta_{zyz} + \beta_{zzy}) \\ +\langle sin^3\theta cos\psi\rangle(\beta_{xyy} + \beta_{yxy} + \beta_{yyx} - \beta_{xzz} - \beta_{zxz} - \beta_{zzx}) \\ +\langle sin^3\theta sin^3\psi\rangle(-\beta_{yyy} + \beta_{xxy} + \beta_{xyx} + \beta_{yxx}) \\ +\langle sin^3\theta cos^3\psi\rangle(\beta_{xxx} - \beta_{xyy} - \beta_{yxy} - \beta_{yyx}) \end{Bmatrix}. \quad \text{(S29)}$$

When the distribution of ψ angle is also isotropic (see Fig. 1(b)), $\langle sin^2\psi\rangle = \langle cos^2\psi\rangle = \frac{1}{2}$ and $\langle sin\psi\rangle = \langle cos\psi\rangle = \langle sin\psi cos\psi\rangle = \langle sin^3\psi\rangle = \langle cos^3\psi\rangle = 0$. Eqn (S26)-(S29) can be simplified into

$$\chi_{ZZZ} = N_s \times$$

$$\begin{Bmatrix} \langle cos^3\theta\rangle(\beta_{zzz}) \\ +\langle sin^2\theta scos\theta\rangle(\beta_{yyz} + \beta_{yzy} + \beta_{zyy} + \beta_{xxz} + \beta_{xzx} + \beta_{zxx})/2 \end{Bmatrix}, \quad \text{(S30)}$$

$$\chi_{ZXX} = \frac{1}{2}N_s \times$$

$$\begin{Bmatrix} \langle sin^2\theta cos\theta\rangle(\beta_{zzz}) + \langle cos\theta\rangle(\beta_{zxx} + \beta_{zyy}) \\ -\langle sin^2\theta cos\theta\rangle(\beta_{yyz} + \beta_{yzy} + \beta_{zyy} + \beta_{xxz} + \beta_{xzx} + \beta_{zxx})/2 \end{Bmatrix}, \quad \text{(S31)}$$

$$\chi_{XZX} = \frac{1}{2} N_s \times$$

$$\begin{Bmatrix} \langle sin^2\theta cos\theta \rangle (\beta_{zzz}) + \langle cos\theta \rangle (\beta_{xzx} + \beta_{yzy}) \\ -\langle sin^2\theta cos\theta \rangle (\beta_{yyz} + \beta_{yzy} + \beta_{zyy} + \beta_{xxz} + \beta_{xzx} + \beta_{zxx})/2 \end{Bmatrix}, \quad \text{(S32)}$$

$$\chi_{XXZ} = \frac{1}{2} N_s \times$$

$$\begin{Bmatrix} \langle sin^2\theta cos\theta \rangle (\beta_{zzz}) + \langle cos\theta \rangle (\beta_{xxz} + \beta_{yyz}) \\ -\langle sin^2\theta cos\theta \rangle (\beta_{yyz} + \beta_{yzy} + \beta_{zyy} + \beta_{xxz} + \beta_{xzx} + \beta_{zxx})/2 \end{Bmatrix}. \quad \text{(S33)}$$

In a non-resonant case, the polarizability are symmetric: $\alpha_{\sigma\rho} = \alpha_{\rho\sigma}$ (see eqn (9)). Hence, $\beta_{\sigma\rho\kappa} = \beta_{\rho\sigma\kappa}$. For $\beta_{xzx} = \beta_{zxx}$ and $\beta_{yzy} = \beta_{yyz}$, $\chi_{XZX} = \chi_{ZXX}$.

S10. Theoretical and experimental SFVS

In ref. [18-23], scientists conducted studies on SFVS of methanol at gas/liquid interfaces. In ref [21], Li et al. presented the absolute ssp and ppp intensities and there are relative intensities in other references. We compare our theoretical results with experiment.[21] In order to compare our computations with other experimental results, we assume that the absolute macroscopic susceptibilities χ_{YYZ} of the strongest ssp peak are the same. Hence, the ssp strongest intensities are proportional to the square of $sin\beta_2$ (see eqn (2)). There is no simple relationship between the ppp intensities and the trigonometric function values of the incident and reflection angles of the lights (see eqn (3)). Therefore, we present the theoretical and experimental ssp spectra in Fig. 2, S5(a)-S7(a) and S9(a), only the theoretical ppp spectra in Fig. S5(b)-S8(b), and the theoretical and experimental ppp spectra in Fig. S9(b). The main differences of the experimental spectra are that their incident angles are somewhat different.

From Fig. 2, S5-S7 and S9, we find that the second strongest peaks of the ssp spectra in ref. [18,22,23], which agree with our computations, are weaker than those of the other

SFVS experiments. The intensities of the visible and IR input lights are different in experiments,[18-24] which may have different interactions of the incident lights with molecules at interfaces and affect molecular properties and orientations. This may be the reason why there are different SFVS at gas/liquid interfaces for the same methanol molecules.

In Fig. S9, we plot the ssp and ppp spectra and display four terms (see eqn (3)) including the influences of the incident and reflection angles of the lights and Lorentz local field corrections. Fig. S9(c) show that the χ_{XXZ} term predominates. Thus, also the xxz and yyz components of the hyperpolarizablities dominate the SFVS intensities. The χ_{XZX} and χ_{ZXX} terms are relatively small and modify the ppp spectra. Form section S9, we know that $\chi_{XZX} = \chi_{ZXX}$. Their corresponding trigonometric function products are respectively 0.2579 and 0.2719 when the incident angles of the IR and Vis lights are 58^o and 45^o, respectively. Therefore, the χ_{XZX} and χ_{ZXX} terms are almost coincident. The χ_{ZZZ} term is very small for its Lorentz local field correction is small with a value of 0.1773. Comparing Fig. 9(b) and 9(a), we find that the ppp spectra are smaller than the ssp ones. The reason is that the trigonometric function values for the χ_{XXZ} terms of the ssp and ppp spectra are 0.8480 and 0.4127, respectively.

Furthermore, we discover that the frequencies calculated by us in theoretical SFVS are smaller than experimental ones (see Fig. 2 and S5-S9), and the computed anharmonic vibrational frequencies are in good agreement with experiments (see Table S1) . The reason is that we apply two different methods to obtain the frequencies: when studying Fermi resonance, we only consider the cubic force constants, which relate the

overtones and combinations of the H-C-H bending modes to the C-H stretching modes, and the other non-diagonal coupling terms are taken to be zero; however, when investigating the anharmonic frequencies, Barone[10] achieves more accurate vibrational frequencies including the quadratic, cubic and quartic force constants contributions of all the normal modes to calculate the diagonal and non-diagonal terms of the anharmonic X matrix.

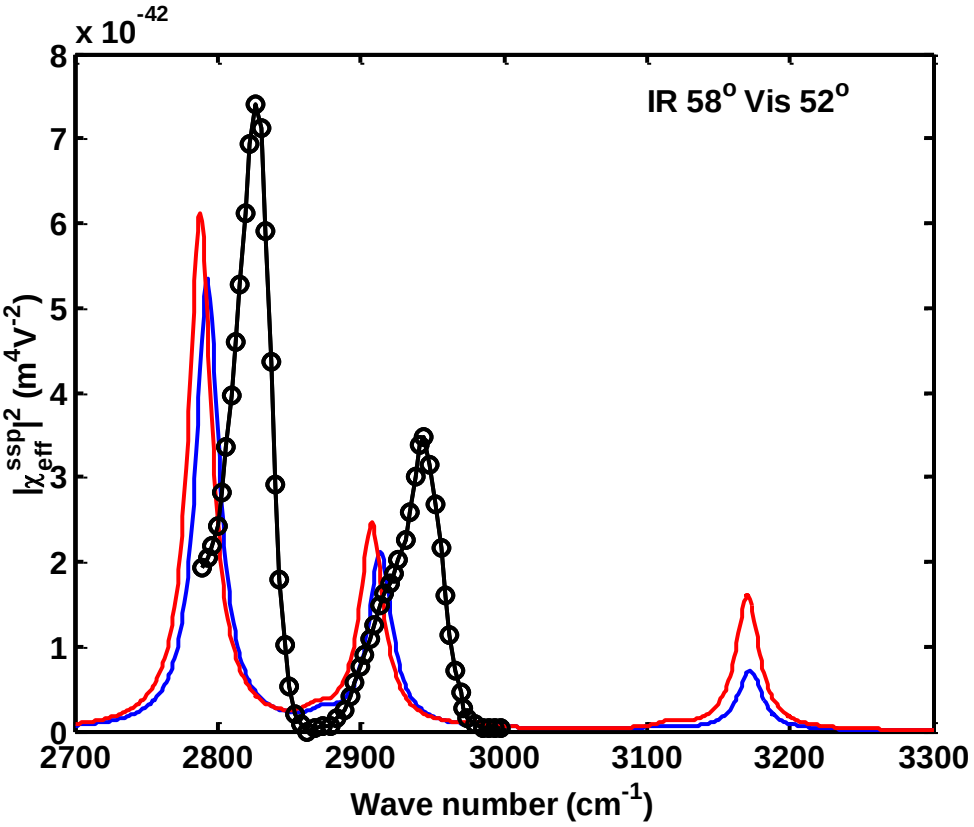

(a)

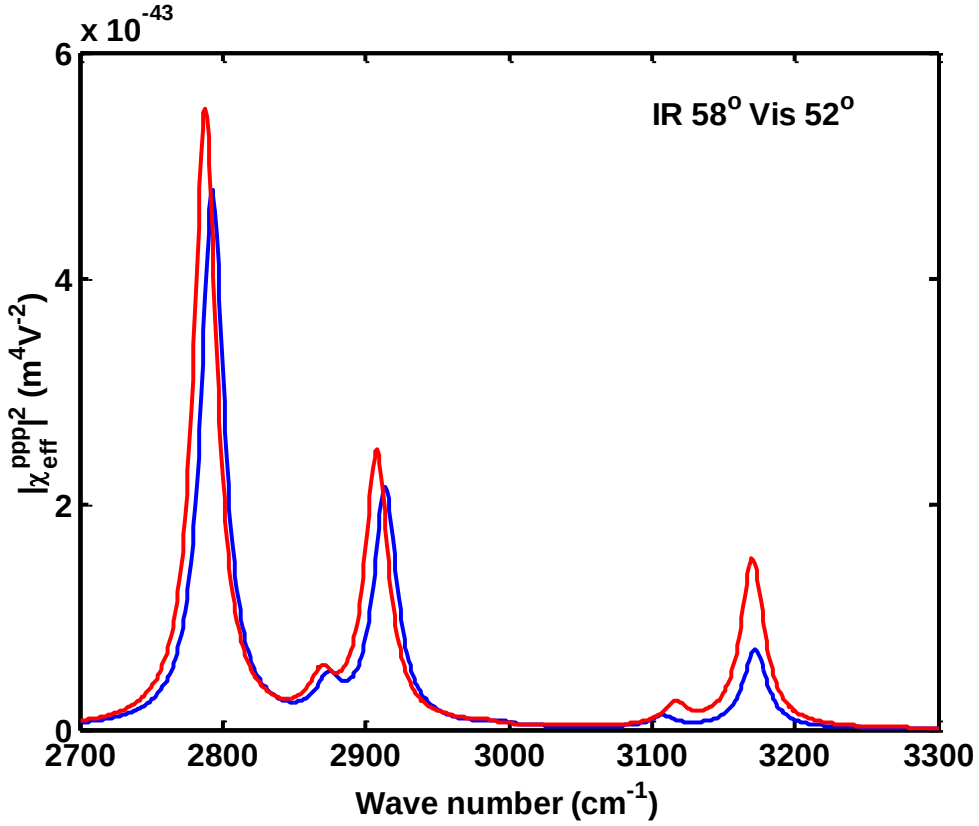

(b)

Fig. S5. The (a) ssp and (b) ppp spectra in gas phase including the contributions of first-order and second-order dipole moment and polarizabilty derivatives (blue), using PCM (red), and the experimental ones (open circles) in ref. [19] when the two incident angles of the IR and Vis lights are 58° and 52°, respectively.

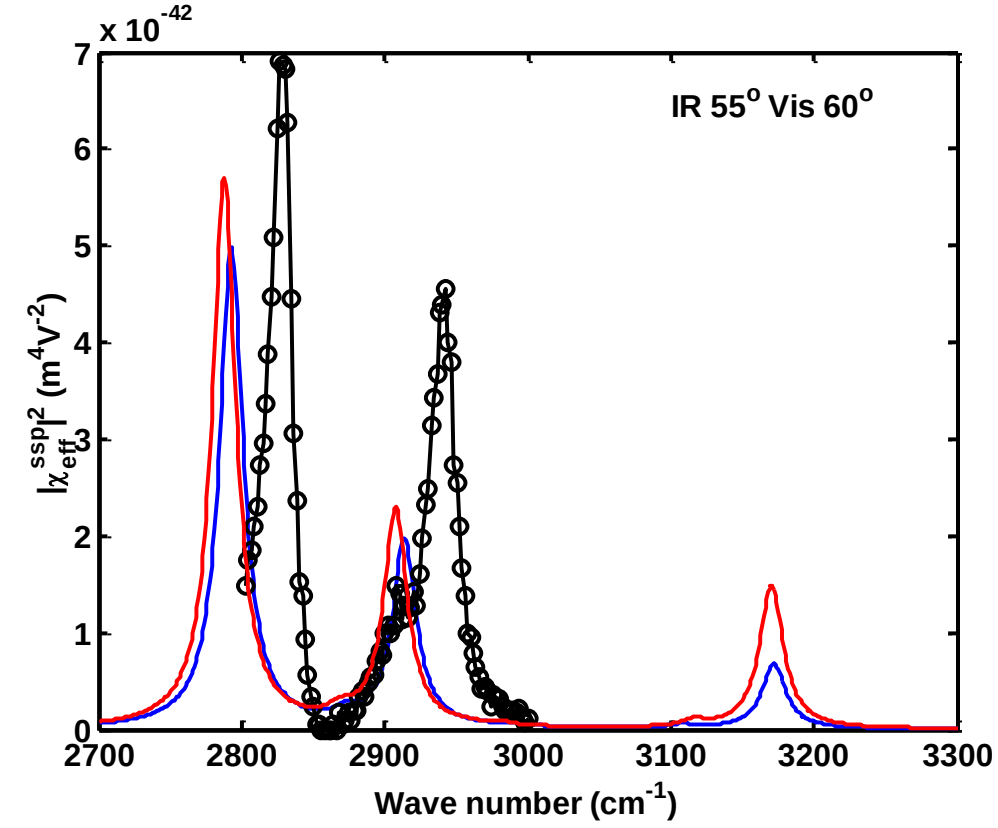
x 10^-42
IR 55° Vis 60°
|χ_eff^ssp|^2 (m^4V^-2)
Wave number (cm^-1)

(a)

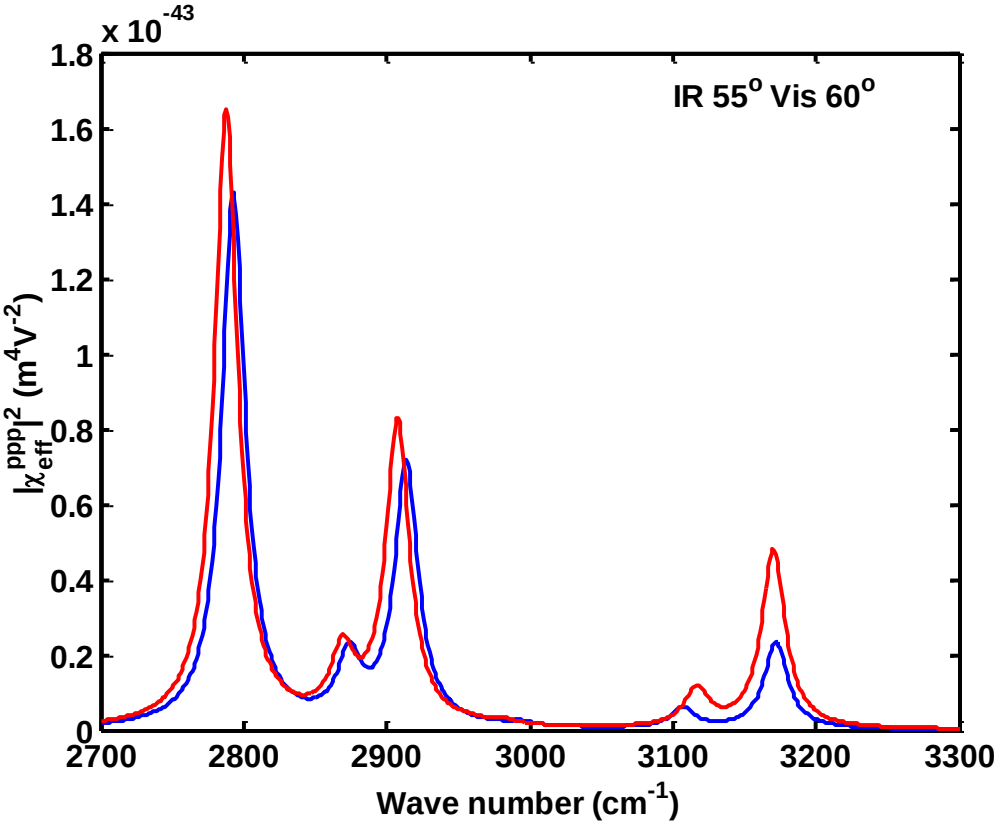
x 10^-43
IR 55° Vis 60°
|χ_eff^ppp|^2 (m^4V^-2)
Wave number (cm^-1)

(b)

Fig. S6. The (a) ssp and (b) ppp spectra in gas phase including the contributions of first-order and second-order dipole moment and polarizabilty derivatives (blue), using PCM (red), and the experimental ones (open circles) in Ref. [20] when the two incident angles of the IR and Vis lights are 55° and 60°, respectively.

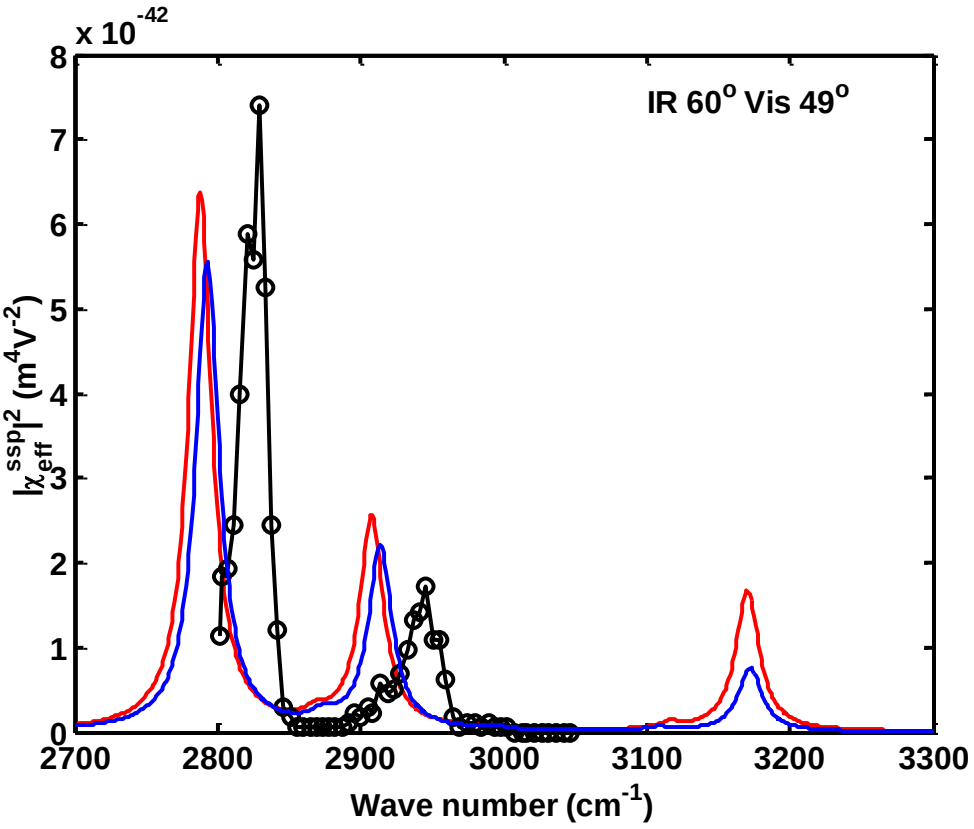

(a)

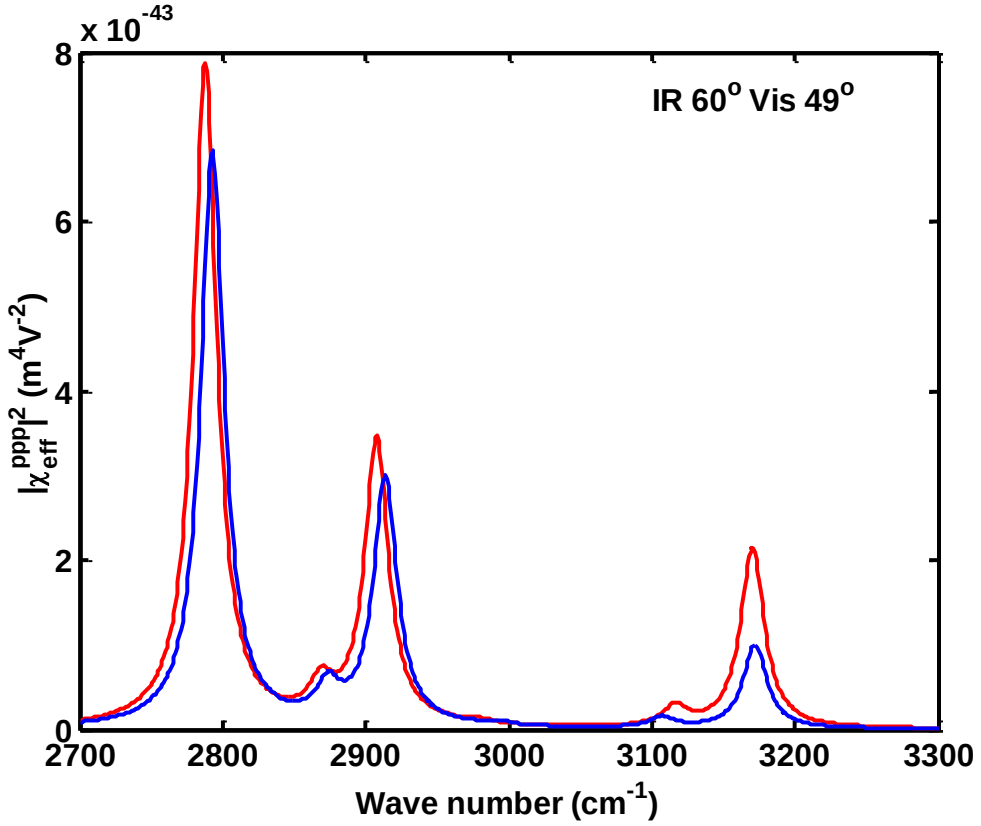

(b)

Fig. S7. The (a) ssp and (b) ppp spectra in gas phase including the contributions of first-order and second-order dipole moment and polarizability derivatives (blue), using PCM (red), and the experimental ones (open circles) in ref. [22] when the two incident angles of the IR and Vis lights are 60° and 49°, respectively.

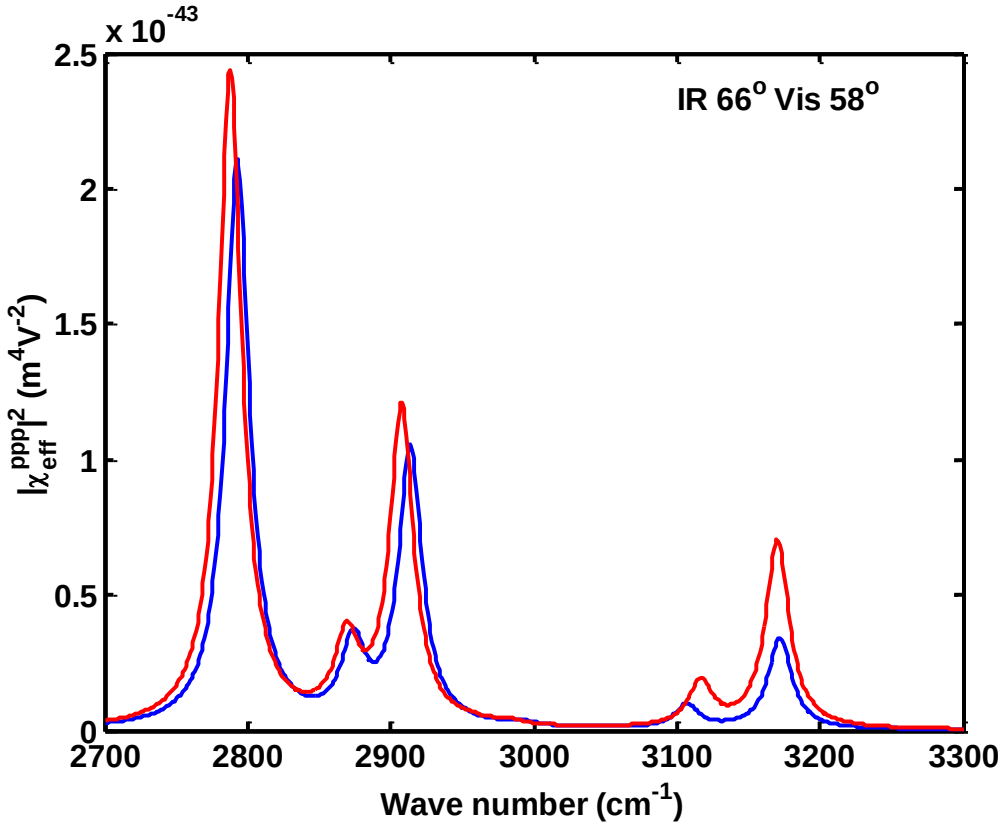

Fig. S8. The ppp spectra in gas phase including the contributions of first-order and second-order dipole moment and polarizability derivatives (blue) and using PCM (red) when the two incident angles of the IR and Vis lights are 66° and 58°, respectively.

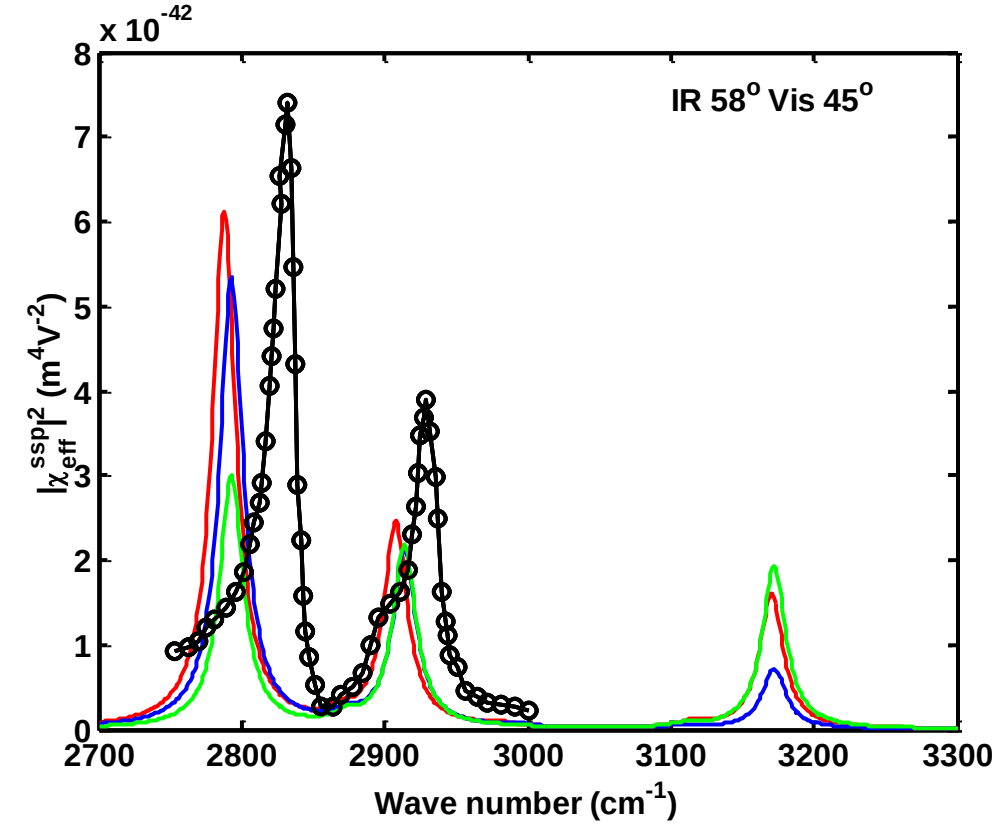
x 10^-42
IR 58° Vis 45°
|χ_eff^ssp|^2 (m^4v^-2)
Wave number (cm^-1)

(a)

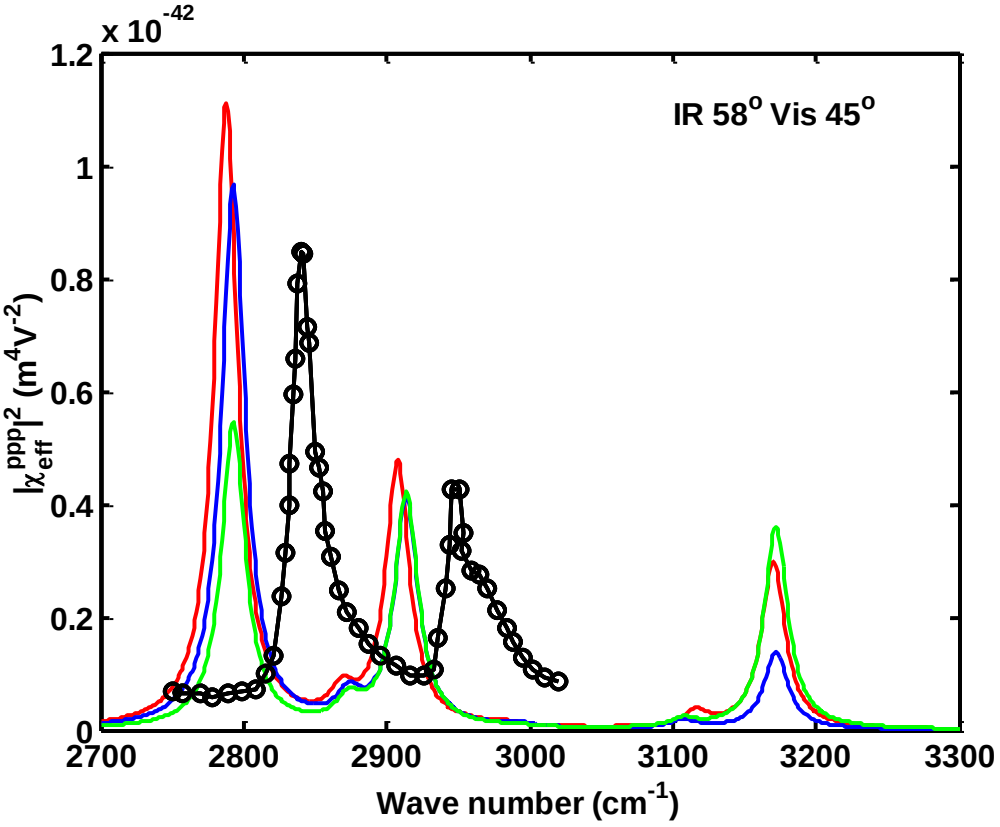
x 10^-42
IR 58° Vis 45°
|χ_eff^ppp|^2 (m^4v^-2)
Wave number (cm^-1)

(b)

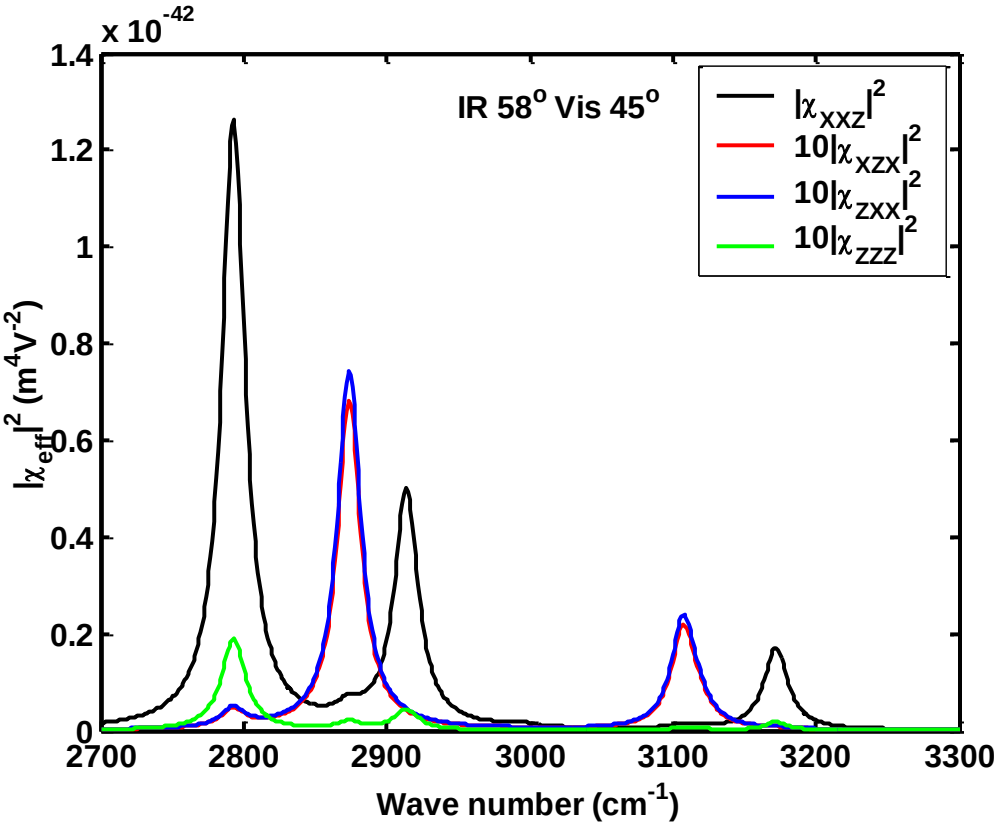

Fig. S9. The (a) ssp and (b) ppp spectra with the contributions of the first-order and second-order dipole moment and polarizability derivatives (blue), without the contributions of second-order derivatives (green) in gas phase, using PCM (red), and the experimental spectra (open circles) in ref. [21], and (c) the four terms that affect the ppp spectra including the influences of the incident and reflection angles of the lights and Lorentz local field corrections in gas phase when the incident angles of the IR and Vis lights are 58° and 45°, respectively.

Table S9 The second-order susceptibilities χ^0 in gas phase and χ^{PCM} (10^{-23}i m^2/V) calculated by PCM for Fermi modes when the IR light is exactly resonant to Fermi vibrational frequencies (cm^{-1}) and the incident angles of the IR and Vis lights are 58° and 45°, respectively

n_F	1_F	2_F	3_F	4_F	5_F	6_F	7_F	8_F	9_F
Frequency	2793	2874	2914	2974	2980	2994	3107	3119	3172
χ^0_{XXZ}	175	-26.0	109	5.28	-0.831	13.1	-14.3	7.81	64.2
χ^0_{XZX}	15.5	67.0	2.43	-0.324	2.13	-0.595	36.8	13.8	3.87
χ^0_{ZXX}	15.5	67.0	2.43	-0.324	2.13	-0.595	36.8	13.8	3.87
χ^0_{ZZZ}	179	52.0	84.6	3.73	1.66	10.9	28.6	21.3	53.0
χ^0_{ssp}	231	-34.3	144	6.95	-1.10	17.3	-18.9	10.3	84.6
χ^0_{ppp}	-98.1	21.8	-63.6	-3.10	0.698	-7.58	12.0	-3.13	-37.0
χ^{PCM}_{ssp}	247	-34.5	155	10.8	-0.381	18.0	5.78	-26.1	126
χ^{PCM}_{ppp}	-105	22.1	-68.4	-4.90	0.244	-7.95	-0.870	16.7	-54.5

References

1 X. Zhuang, P. B. Miranda, D. Kim and Y. R. Shen, *Phys. Rev. B*, 1999, **59**, 12632-12640.

2 M. A. Belkin, T. A. Kulakov, K. H. Ernst, L. Yan and Y. R. Shen, *Phys. Rev. Lett.*, 2000, **85**, 4474-4477.

3 A. J. Moad and G. J. Simpson, *J. Phys. Chem. B*, 2004, **108**, 3548-3562.

4 R.-h. Zheng, W.-m. Wei, Y.-y. Jing, H. Liu and Q. Shi, *J. Phys. Chem. C*, 2013, **117**, 11117-11123.

5 T. Yanai, D. P. Tew and N. C. Handy, *Chem. Phys. Lett.*, 2004, **393**, 51-57.

6 J. Tomasi, B. Mennucci and R. Cammi, *Chem. Rev.*, 2005, **105**, 2999-3093.

7 T. Shimanouchi, *National Bureau of Standards*, 1972, **1**, 1-160.

8 J. E. Bertie and S. L. L. Zhang, *J. Mol. Struct.*, 1997, **413-414**, 333-363.

9 V. Barone and C. Minichino, *J. Mol. Struct.-Theochem*, 1995, **330**, 365-376.

10 V. Barone, *J. Chem. Phys.*, 2005, **122**, 014108.

11 M. J. Frisch, G. W. Trucks, H. B. Schlegel, G. E. Scuseria, M. A. Robb, J. R. Cheeseman, G. Scalmani, V. Barone, G. A. Petersson, H. Nakatsuji, M. Caricato, A. V. Marenich, J. Bloino, B. G. Janesko, R. Gomperts, B. Mennucci, H. P. Hratchian, J. V. Ortiz, A. F. Izmaylov, J. L. Sonnenberg, D. Williams-Young, F. Ding, F. Lipparini, F. Egidi, J. Goings, B. Peng, A. Petrone, T. Henderson, D. Ranasinghe, V. G. Zakrzewski, J. Gao, N. Rega, G. Zheng, W. Liang, M. Hada, M. Ehara, K. Toyota, R. Fukuda, J. Hasegawa, M. Ishida, T. Nakajima, Y. Honda, O. Kitao, H. Nakai, T. Vreven, K. Throssell, J. A. J. Montgomery, J. E. Peralta, F. Ogliaro, M. Bearpark, J. J. Heyd, E. Brothers, K. N. Kudin, V. N. Staroverov, R. Kobayashi, J. Normand, K. Raghavachari, A. Rendell, J. C. Burant, S. S. Iyengar, J. Tomasi, M. Cossi, J. M. Millam, M. Klene, C. Adamo, R. Cammi, J. W. Ochterski, R. L. Martin, K. Morokuma, O. Farkas, J. B. Foresman and D. J. Fox, *Gaussian 16, Revision A.03, Gaussian, Inc., Wallingford CT*, 2016.

12 A. Bagchi, R. G. Barrera and R. Fuchs, *Phys. Rev. B*, 1982, **25**, 7086-7096.

13 P. X. Ye and Y. R. Shen, *Phys. Rev. B*, 1983, **28**, 4288-4294.

14 A. Austin, G. A. Petersson, M. J. Frisch, F. J. Dobek, G. Scalmani and K. Throssell, *J. Chem. Theory Comput.*, 2012, **8**, 4989-5007.

15 R.-H. Zheng, W.-M. Wei, H. Liu, Y.-Y. Jing, B.-Y. Wang and Q. Shi, *J. Chem. Phys.*, 2014, **140**, 104702.

16 D. van derSpoel, E. Lindahl, B. Hess, A. R. van Buuren, E. Apol, P. J. Meulenhoff,

D. P. Tieleman, A. L. T. M. Sijbers, K. A. Feenstra, R. van Drunen and H. J. C. Berendsen, *Gromacs User Manual*, 2010, **version 4.5**.

17 D. J. Adams and G. S. Dubey, *J. Comput. Phys.*, 1987, **72**, 156-176.

18 T. Ishiyama, V. V. Sokolov and A. Morita, *J. Chem. Phys.*, 2011, **134**, 024509.

19 R. Superfine, J. Y. Huang and Y. R. Shen, *Phys. Rev. Lett.*, 1991, **66**, 1066-1069.

20 R. Lu, W. Gan, B. H. Wu, Z. Zhang, Y. Guo and H. F. Wang, *J. Phys. Chem. B*, 2005, **109**, 14118-14129.

21 X. Li, J. Liu, K. Zhang, Y. Zhang, Y. Zhang, R. Zheng, Q. Shi, Y. Guo and Z. Lu, *J. Phys. Chem. C*, 2019, **123**, 12975-12983.

22 J. H. Sung, K. Park and D. Kim, *J. Phys. Chem. B*, 2005, **109**, 18507-18514.

23 G. Ma and H. C. Allen, *J. Phys. Chem. B*, 2003, **107**, 6343-6349.

24 P. Guyotsionnest, J. H. Hunt and Y. R. Shen, *Phys. Rev. Lett.*, 1987, **59**, 1597-1600.